Hu, Xuerong; Du, Luojun; Wang, Yadong; Lahtinen, Jouko; Yao, Lide; Ren, Zhaoyu; Sun, Zhipei

Raman fingerprints and exciton-phonon coupling in 2D ternary layered semiconductor InSeBr

Raman fingerprints and exciton-phonon coupling in 2D ternary layered semiconductor InSeBr

Xuerong Hu [iD], Luojun Du [iD], Yadong Wang [iD], Jouko Lahtinen [iD], Lide Yao [iD], Zhaoyu Ren, and Zhipei Sun [iD]

View Online   Export Citation   CrossMark

ARTICLES YOU MAY BE INTERESTED IN

Terahertz emission from in-plane and out-of-plane dipoles in layered SnS_2 crystal
Applied Physics Letters **116**, 161901 (2020); https://doi.org/10.1063/5.0004701

High performance $CsPbBr_3$ quantum dots photodetectors by using zinc oxide nanorods arrays as an electron-transport layer
Applied Physics Letters **116**, 162103 (2020); https://doi.org/10.1063/5.0005464

Low voltage thin film transistors based on solution-processed In_2O_3:W. A remarkably stable semiconductor under negative and positive bias stress
Applied Physics Letters **116**, 163505 (2020); https://doi.org/10.1063/1.5142699

Raman fingerprints and exciton-phonon coupling in 2D ternary layered semiconductor InSeBr

Xuerong Hu,[1,2] (iD) Luojun Du,[2,a)] (iD) Yadong Wang,[2] (iD) Jouko Lahtinen,[3] (iD) Lide Yao,[3] (iD) Zhaoyu Ren,[1,b)] (iD) and Zhipei Sun[2,4] (iD)

AFFILIATIONS

[1]Institute of Photonics and Photon Technology, Northwest University, Xi'an 710069, China
[2]Department of Electronics and Nanoengineering, Aalto University, Espoo 02150, Finland
[3]Department of Applied Physics, Aalto University, Espoo 02150, Finland
[4]QTF Centre of Excellence, Department of Applied Physics, Aalto University, Espoo 00076, Finland

a)luojun.du@aalto.fi
b)rzy@nwu.edu.cn

ABSTRACT

Compared to other two-dimensional (2D) crystals with single or binary elements, 2D ternary layered materials have unique physical properties for potential applications due to the stoichiometric variation and synergistic effect. Here, we report the first investigation of lattice dynamics and interactions between the exciton and lattice degrees of freedom in a 2D ternary semiconductor: indium-selenide-bromide (InSeBr). Via linear polarization resolved Raman scattering measurements, we uncover three Raman modes in few-layer InSeBr, including two A_{1g} and one E_g modes. Moreover, through the combination of temperature-dependent Raman scattering experiments and theoretical calculations, we elucidate that few-layer InSeBr would harbor strong coupling between excitons and phonons. Our results may provide a firm basis for the development and engineering of potential optoelectronic devices based on 2D ternary semiconductors.

Published under license by AIP Publishing. https://doi.org/10.1063/1.5143119

Since the discovery of graphene,[1] two-dimensional (2D) van der Waals (vdW) materials have sparked significant attention and initiated the promising era of basic scientific research and modern technological advances because of their unique electrical, optical, and magnetic properties.[2–9] For example, 2D honeycomb lattices, such as gapped graphene and transition metal dichalcogenides (TMDCs), reinvigorate the field of valleytronics and provide an unprecedented platform to address and control the valley degrees of freedom for information storage and encoding.[3,8,10–14] Until now, the research of 2D materials is mainly focused on single (for example, graphene,[1,15] black phosphorus,[16,17] and silicene[18,19]) and binary elemental crystals (such as TMDCs,[3,20,21] GaSe,[22] GeSe,[23] and InSe[24,25]).

Strikingly, the recently emerging 2D ternary vdW materials have attracted increasing attention due to their enchanting physical properties for potential applications since the inclusion of a third element offers one more degree of freedom to control the stoichiometry and tune the physical properties.[26–31] For instance, the ferromagnetic transition temperature of itinerant vdW ferromagnet Fe_3GeTe_2 can be tuned from 150 K to 220 K by changing the Fe occupancy.[32] Few-layer 2D ternary $Ga_2In_4S_9$ exhibits appealing ultraviolet light detection

performance with an outstanding responsivity of 111.9 AW^{-1}, an excellent external quantum efficiency of 3.85×10^4%, and a specific detectivity of 2.25×10^4 Jones.[30] Ultrathin Bi_2O_2Se nanosheets provide high electron mobility ($\approx 30\,000$ cm^2 V^{-1} s^{-1} at low temperature), a moderate bandgap (≈ 0.8 eV), a near-ideal subthreshold swing value (≈ 65 mV dec^{-1}), and excellent environmental stability, offering an unprecedented platform toward high-performance optoelectronic devices at the nanoscale.[27,33–35] In addition, 2D ternary materials can harbor the synergistic effect between various components, giving rise to fascinating phenomena and functionalities. For example, by adding Fe^{3+} ions into CuSe, forming CuFeSe nanosheets, the intrinsic properties and performance could be highly modified, which shows great promise of ternary metal chalcogenide nanosheets for chemotherapy of cancer and exhibits excellent anticancer efficacy.[36]

The studies of 2D ternary vdW materials are still at the infant stage, and so it is important to search for potential ternary vdW materials and investigate the corresponding basic physical properties, such as phonon–phonon and electron-phonon coupling, which play a vital role in a wide range of applications in condensed matter physics.[37–41] InSeBr, a ternary layered semiconductor with a deep-red color and

energy bandgap in the visible region,[42,43] would open a promising paradigm for a variety of potential applications in the fields of electronics and optoelectronics. However, the properties of InSeBr are largely unexplored. Here, we systematically and comprehensively investigate the phonon behaviors and exciton-phonon coupling in few-layer InSeBr. We uncover the Raman fingerprints (two A_{1g} and one E_g) of few-layer InSeBr by polarized Raman scattering experiments. Moreover, the temperature-dependent Raman measurements show that the evolution of phonon lifetimes with temperature strongly diverges from the anharmonic model. In conjunction with photoluminescence (PL) spectra and theoretical calculations, we elucidate that the increase in phonon linewidths with decreasing temperature can be understood as the strong coupling between phonons and excitons in few-layer InSeBr.

Ternary InSeBr is a layered material with weak vdW interaction and reveals p-type semiconducting behavior.[43,44] Each layer is three-atom thick, where the In atoms of the middle sheet are sandwiched between a single layer of Se and Br atoms in a trigonal structure (a, b = 0.40 nm, c = 1.88 nm, and α, $\beta = 90°$, $\gamma = 120°$), as shown in Fig. 1(a) (top view) and 1(b) (side view).[42,43] In order to confirm chemical composition and quality of the bulk sample (2D Semiconductors), we performed the x-ray photoelectron spectroscopy (XPS) measurements (see supplementary material S1). The binding energies of In $3d_{5/2}$ and In $3d_{3/2}$ correspond to 452.4 eV and 444.9 eV, respectively [Fig. 1(c)]. The Se 3d and Br 3d peaks are deconvoluted to show the $3d_{5/2}$ and $3d_{3/2}$ doublets at 55.5 eV and 54.7 eV for Se and

69.1 eV and 70.2 eV for Br [Figs. 1(d) and 1(e)].[45,46] High-resolution transmission electron microscopy (HRTEM) imaging was performed to inspect the crystal quality and orientation of the layered InSeBr (see supplementary material S2). The HRTEM image and corresponding fast Fourier transformation (FFT) pattern in Fig. 1(f) show that the layered InSeBr has a good single-crystalline structure. The inter-planar distance (2 Å) of the (200) plane can be recognized and measurable in Fig. 1(g), which is in good agreement with the optimized in-plane lattice constants in the first-principles calculation.

For the InSeBr crystal, it belongs to the D_{3d}^5 ($R\bar{3}m$) space group.[43] According to group theory, the symmetries of Raman active modes and the corresponding Raman tensors (R) are described as follows:[47]

$$A_{1g} : \begin{pmatrix} a & 0 & 0 \\ 0 & a & 0 \\ 0 & 0 & b \end{pmatrix}; \quad E_g : \begin{pmatrix} 0 & c & d \\ c & 0 & 0 \\ d & 0 & 0 \end{pmatrix} \begin{pmatrix} c & 0 & 0 \\ 0 & -c & d \\ 0 & d & 0 \end{pmatrix}.$$

For the non-resonant Raman scattering intensity of a Raman active mode in a crystal, it can be calculated within the Placzek approximation and expressed by the Raman tensor as $I \propto |e_i \cdot R \cdot e_s|^2$, where e_i and e_s are the polarization vectors of the incident and scattered light, respectively.[47] In the back-scattering configuration, e_i and e_s are within the xy plane. Using the tabulated Raman tensors, we can know that the intensity of A_{1g} mode is maximum (minimum) when the incident light is parallel (perpendicular) to the scattered light, while the intensity of E_g is independent of the angle θ between e_i and e_s.

2D InSeBr flakes were mechanically exfoliated onto a silicon wafer with a 285 nm silica layer (see supplementary material S3).[1] An optical microscopy image of few-layer InSeBr is shown in Fig. S3 (supplementary material) with a strongly layer-dependent optical contrast, which indicates the characteristics of the layered structure. Figure 2(a) shows the topography of atomic force microscopy (AFM) scanning (see supplementary material S3). The height profiles indicate that the thickness of the majority part of the flake is ~6 nm, corresponding to ~10 layers [Fig. 2(b)]. In order to confirm the Raman fingerprints of InSeBr, we first performed the unpolarized Raman scattering with three laser excitation wavelengths (488, 532, and 633 nm) in ambient conditions, as shown in Fig. 2(c). Three non-resonant Raman modes are evidently observed (indicated by the blue dashed vertical lines). Through
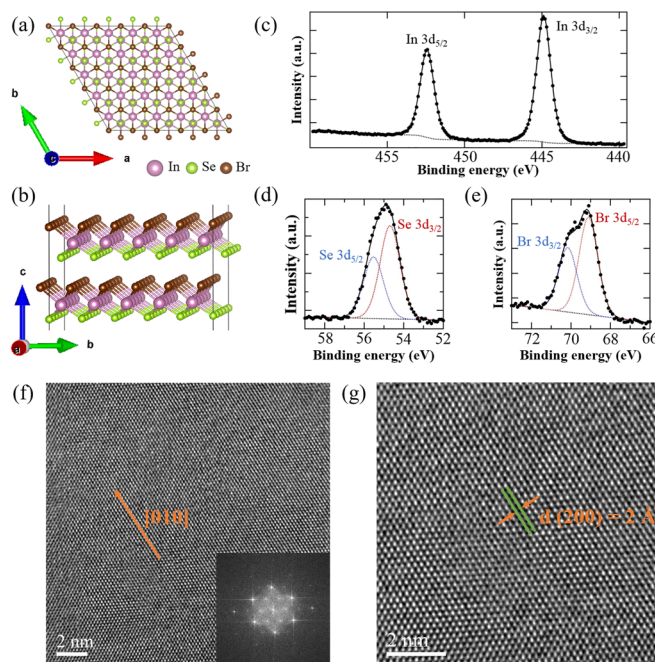

FIG. 1. InSeBr structures and characterization. (a) Top view and (b) side view of the crystal structure of few-layer InSeBr. In atoms are purple, Se atoms are green, and Br atoms are brown. XPS spectra of (c) In, (d) Se, and (e) Br in InSeBr sheets. (f) HRTEM image of a few-layer InSeBr flake from the [001] zone axis, indicating the [010] preferential crystal orientation. Inset: corresponding fast Fourier transformation image. (g) The enlarged HRTEM image.

FIG. 2. InSeBr flake and its unpolarized Raman response at different wavelengths. (a) AFM image of the InSeBr flake. (b) Height profiles taken along the white line in Fig. 2(a). (c) Unpolarized Raman spectra of InSeBr and the SiO$_2$ substrate obtained with 488, 532, and 633 nm laser excitation, respectively. The spectra are normalized and vertically offset for clarify. (d) The Lorentz fitting of the unpolarized Raman spectra of InSeBr with 488 nm laser excitation.

Lorentz fitting of the results at 488 nm [Fig. 2(d)] and 633 nm [Fig. S4] (supplementary material), it can be known that these three peaks are identified at 111, 170, and 210 cm^{-1}, respectively.

 To further clarify the symmetry of phonons, we performed the linear polarization resolved Raman scattering measurements. More details on the measurement methods can be found in supplementary material S4. Figure 3(a) presents the Raman spectra excited by linearly polarized light and collected in co-polarized (linearly parallel, red) or cross-polarized (linearly perpendicular, black) geometry. The evolution of Raman intensities with the angle θ between e_i and e_s is presented in Fig. 3(b). For the mode of 111 cm^{-1}, the intensities are independent of the angle θ, indicating the symmetry of E_g. In stark contrast, the intensities of the other two modes (170 and 210 cm^{-1}) are strongly dependent on the angle θ and exhibit cosine behaviors (red lines), demonstrating the A_g symmetry.

 After the identification of lattice dynamics in InSeBr, we performed temperature-dependent measurements (see supplementary material S4) to investigate the coupling between phonons and other elementary excitations, which provide a firm basis for many physical phenomena, such as the formation of Cooper pairs, carrier dynamics, and spin-Seebeck effect.[29,37,38,48] Since A_{1g} of 170 cm^{-1} possesses the largest intensity, we focus on this mode to study the temperature effects. Figure 4(a) shows the temperature-dependent Raman spectra. The temperature-driven evolution of phonon frequencies (ω) and the full width at half maximum (FWHM) for the A_{1g} mode at ~170 cm^{-1} are presented in Figs. 4(b) and 4(c), respectively. Usually, the temperature-dependent phonon frequencies (linewidths) can be described in terms of the anharmonic model and increase (decrease) with decreasing temperature.[29,49] For the phonon frequencies, both the 170 cm^{-1} mode of InSeBr and 520 cm^{-1} mode of silicon exhibit the monotonous blue-shift when temperature decreases, in fair agreement with the anharmonic model. For the FWHM, the 520 cm^{-1} mode of silicon can also be well described with the anharmonic model and decreases with decreasing temperature. In stark contrast, the FWHM for the 170 cm^{-1} mode of InSeBr increases with decreasing

FIG. 4. (a) Temperature-dependent Raman spectra of the InSeBr flake and the silicon substrate reference. (b) Raman peak positions and (c) FWHM of the 170 cm^{-1} Raman mode of InSeBr (left vertical axis) and 520 cm^{-1} Raman mode of the silicon reference (right vertical axis) as a function of temperature. (d) Band structures of monolayer, (e) bilayer, and (f) bulk InSeBr. (g) PL spectra of InSeBr at different temperatures.

temperature, strongly diverging from the standard anharmonic model. This phenomenon indicates another phonon relaxation pathway besides the symmetric anharmonic decay (i.e., decay into a pair of acoustic modes with identical frequencies and opposite momenta) and a strong coupling between the phonon and other elementary excitations. Since InSeBr is a non-magnetic material, such anomalous temperature-dependent FWHM behavior cannot come from the magnetic elementary excitations.[29,48]

 Due to the reduced screening effect in 2D materials, the coupling between phonons and excitons would be significantly enhanced.[38,40] We expect that the anomalous phenomenon of FWHM for the 170 cm^{-1} mode of InSeBr may stem from the exciton-phonon interaction, which can lead to the enhancement of FWHM.[50] To confirm this point of view, we first performed first-principles calculations. A detailed description of the calculation methods is given in supplementary material S5. Figures 4(d)–4(f) show the electronic band structure of the monolayer, bilayer, and bulk InSeBr. For the monolayer, the direct bandgap at the Γ point is 1.90 eV and the indirect bandgap between Γ and M points is 1.42 eV. Therefore, monolayer InSeBr is an indirect bandgap semiconductor, and the difference between direct and indirect bandgaps is 0.48 eV. With the increasing layer number, the direct bandgap, indirect bandgap, and bandgap differences for the bilayer (bulk) are 1.67 eV (1.47 eV), 1.23 eV (1.34 eV), and 0.44 eV (0.13 eV), respectively. Evidently, the bandgap difference between direct and indirect bandgaps decreases with the increasing layer number, being akin to the case of InSe.[24,51] As a consequence, multi-layer InSeBr is a nearly direct bandgap semiconductor and would harbor strong exciton-phonon coupling. Figure 4(g) shows the temperature-dependent PL spectra. A prominent peak around 2 eV can be clearly observed, which corresponds to the direct bandgap and is in good agreement with the first-principles theoretical prediction and the reflection spectrum in Fig. S6 (see supplementary material S6). Remarkably, the PL intensity increases with the decreasing temperature, leading to the significantly enhanced exciton-phonon interactions and FWHM of phonons.

 In summary, we investigated the Raman fingerprints and exciton-phonon coupling of few-layer ternary InSeBr flakes by
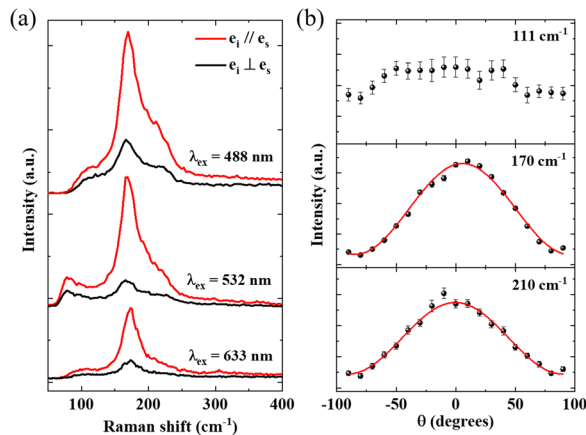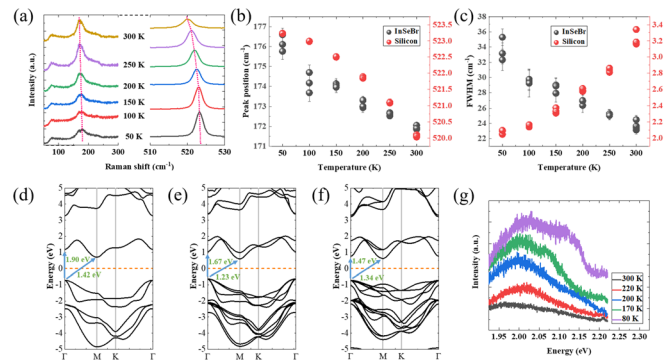

FIG. 3. Linearly polarized Raman responses of InSeBr. (a) Raman spectra of InSeBr obtained in the parallel and cross polarization conditions with 488, 532, and 633 nm excitation. (b) Peak intensity changes with the angle between incident (wavelength of 488 nm) and scattered light polarization. The spectral resolution is about 1 cm^{-1}. All the spectra are normalized and vertically offset for clarify.

theoretical calculations and experimental studies. InSeBr is a layered semiconductor with a layer-dependent bandgap in the visible region ranging from 2.04 eV (bulk) to 2.12 eV (monolayer). Three Raman modes (two A_{1g} at 170 cm^{-1} and 210 cm^{-1} and one E_g at 111 cm^{-1}) are confirmed by polarization-dependent Raman spectra with different laser wavelengths (488 nm, 532 nm, and 633 nm). Temperature-dependent Raman scattering shows that the FWHM of phonons in InSeBr strongly diverges from the standard anharmonic model. In conjunction with theoretical calculations and temperature-dependent PL spectra, we uncover the strong exciton-phonon coupling in few-layer InSeBr flakes. This work exhibits a detailed study of the phonon properties and exciton-phonon interaction, paving the way toward the understanding and engineering of potential optoelectronic applications on 2D ternary semiconductors.

See the supplementary material for XPS characterization, HRTEM characterization, sample preparation, AFM characterization, Raman and PL characterization, theoretical calculations, and reflection characterization.

REFERENCES

[1] K. S. Novoselov, A. K. Geim, S. V. Morozov, D. Jiang, Y. Zhang, S. V. Dubonos, I. V. Grigorieva, and A. A. Firsov, Science **306**, 666 (2004).

[2] K. S. Novoselov, A. Mishchenko, A. Carvalho, and A. H. C. Neto, Science **353**, aac9439 (2016).

[3] K. F. Mak, D. Xiao, and J. Shan, Nat. Photonics **12**, 451 (2018).

[4] X. Zhang, X. F. Qiao, W. Shi, J. B. Wu, D. S. Jiang, and P. H. Tan, Chem. Soc. Rev. **44**, 2757 (2015).

[5] Z. Sun, A. Martinez, and F. Wang, Nat. Photonics **10**, 227 (2016).

[6] C. Jin, E. Y. Ma, O. Karni, E. C. Regan, F. Wang, and T. F. Heinz, Nat. Nanotechnol. **13**, 994 (2018).

[7] C. Gong and X. Zhang, Science **363**, eaav4450 (2019).

[8] X. Xu, W. Yao, D. Xiao, and T. F. Heinz, Nat. Phys. **10**, 343 (2014).

[9] P. Luo, F. Zhuge, Q. Zhang, Y. Chen, L. Lv, Y. Huang, H. Li, and T. Zhai, Nanoscale Horiz. **4**, 26 (2019).

[10] K. F. Mak, K. He, J. Shan, and T. F. Heinz, Nat. Nanotechnol. **7**, 494 (2012).

[11] H. Zeng, J. Dai, W. Yao, D. Xiao, and X. Cui, Nat. Nanotechnol. **7**, 490 (2012).

[12] L. Du, Q. Zhang, B. Gong, M. Liao, J. Zhu, H. Yu, R. He, K. Liu, R. Yang, D. Shi, L. Gu, F. Yan, G. Zhang, and Q. Zhang, Phys. Rev. B **97**, 115445 (2018).

[13] L. Du, Q. Zhang, T. Zhang, Z. Jia, J. Liang, G. B. Liu, R. Yang, D. Shi, J. Xiang, K. Liu, Z. Sun, Y. Yao, Q. Zhang, and G. Zhang, Phys. Rev. B **100**, 161404 (2019).

[14] E. J. Sie, J. W. McIver, Y. H. Lee, L. Fu, J. Kong, and N. Gedik, Nat. Mater. **14**, 290 (2015).

[15] J. Yan, Y. Zhang, P. Kim, and A. Pinczuk, Phys. Rev. Lett. **98**, 166802 (2007).

[16] L. Li, Y. Yu, G. J. Ye, Q. Ge, X. Ou, H. Wu, D. Feng, X. H. Chen, and Y. Zhang, Nat. Nanotechnol. **9**, 372 (2014).

[17] F. Xia, H. Wang, J. C. M. Hwang, A. H. C. Neto, and L. Yang, Nat. Rev. Phys. **1**, 306 (2019).

[18] L. Tao, E. Cinquanta, D. Chiappe, C. Grazianetti, M. Fanciulli, M. Dubey, A. Molle, and D. Akinwande, Nat. Nanotechnol. **10**, 227 (2015).

[19] F. Liu, C. C. Liu, K. Wu, F. Yang, and Y. Yao, Phys. Rev. Lett. **111**, 066804 (2013).

[20] A. Splendiani, L. Sun, Y. Zhang, T. Li, J. Kim, C. Y. Chim, G. Galli, and F. Wang, Nano Lett. **10**, 1271 (2010).

[21] G. B. Liu, D. Xiao, Y. Yao, X. Xu, and W. Yao, Chem. Soc. Rev. **44**, 2643 (2015).

[22] X. Zhou, J. Cheng, Y. Zhou, T. Cao, H. Hong, Z. Liao, S. Wu, H. Peng, K. Liu, and D. Yu, J. Am. Chem. Soc. **137**, 7994 (2015).

[23] X. Hu, P. Huang, K. Liu, B. Jin, X. Zhang, X. Zhang, X. Zhou, and T. Zhai, ACS Appl. Mater. Interfaces **11**, 23353 (2019).

[24] D. A. Bandurin, A. V. Tyurnina, G. L. Yu, A. Mishchenko, V. Zólyomi, S. V. Morozov, R. K. Kumar, R. V. Gorbachev, Z. R. Kudrynskyi, Z. Pezzini, Z. D. Kovalyuk, U. Zeitler, K. S. Novoselov, A. Patanè, L. Eaves, I. V. Grigorieva, V. I. Fal'ko, A. K. Geim, and Y. Cao, Nat. Nanotechnol. **12**, 223 (2017).

[25] Z. Yang, W. Jie, C. H. Mak, S. Lin, H. Lin, X. Yang, F. Yan, S. P. Lau, and J. Hao, ACS Nano **11**, 4225 (2017).

[26] T. Gao, Q. Zhang, L. Li, X. Zhou, L. Li, H. Li, and T. Zhai, Adv. Opt. Mater. **6**, 1800058 (2018).

[27] J. Wu, H. Yuan, M. Meng, C. Chen, Y. Sun, Z. Chen, W. Dang, C. Tan, Y. Liu, J. Yin, Y. Zhou, S. Huang, H. Q. Xu, Y. Cui, H. Y. Hwang, Z. Liu, Y. Chen, B. Yan, and H. Peng, Nat. Nanotechnol. **12**, 530 (2017).

[28] Y. Deng, Y. Yu, Y. Song, J. Zhang, N. Z. Wang, Z. Sun, Y. Yi, Y. Z. Wu, S. Wu, J. Zhu, J. Wang, X. H. Chen, and Y. Zhang, Nature **563**, 94 (2018).

[29] L. Du, J. Tang, Y. Zhao, X. Li, R. Yang, X. Hu, X. Bai, X. Wang, K. Watanabe, T. Taniguchi, D. Shi, G. Yu, X. Bai, T. Hasan, G. Zhang, and Z. Sun, Adv. Funct. Mater. **29**, 1904734 (2019).

[30] F. Wang, T. Gao, Q. Zhang, Z. Y. Hu, B. Jin, L. Li, X. Zhou, H. Li, G. V. Tendeloo, and T. Zhai, Adv. Mater. **31**, 1806306 (2019).

[31] Z. Fei, B. Huang, P. Malinowski, W. Wang, T. Song, J. Sanchez, W. Yao, D. Xiao, X. Zhu, A. F. May, W. Wu, D. H. Cobden, J. H. Chu, and X. Xu, Nat. Mater. **17**, 778 (2018).

[32] A. F. May, S. Calder, C. Cantoni, H. Cao, and M. A. McGuire, Phys. Rev. B **93**, 014411 (2016).

[33] J. Li, Z. Wang, Y. Wen, J. Chu, L. Yin, R. Cheng, L. Lei, P. He, C. Jiang, L. Feng, and J. He, Adv. Funct. Mater. **28**, 1706437 (2018).

[34] J. Wu, Y. Liu, Z. Tan, C. Tan, J. Yin, T. Li, T. Tu, and H. Peng, Adv. Mater. **29**, 1704060 (2017).

[35] Q. Fu, C. Zhu, X. Zhao, X. Wang, A. Chaturvedi, C. Zhu, X. Wang, Q. Zeng, J. Zhou, F. Liu, B. K. Tay, H. Zhang, S. J. Pennycook, and Z. Liu, Adv. Mater. **31**, 1804945 (2019).

[36] X. Jiang, Y. Han, H. Zhang, H. Liu, Q. Huang, T. Wang, Q. Sun, and Z. Li, ACS Appl. Mater. Interfaces **10**, 43396 (2018).

[37] C. Jin, J. Kim, J. Suh, Z. Shi, B. Chen, X. Fan, M. Kam, K. Watanabe, T. Taniguchi, S. Tongay, A. Zettl, J. Wu, and F. Wang, Nat. Phys. **13**, 127 (2017).

[38] L. Du, M. Liao, J. Tang, Q. Zhang, H. Yu, R. Yang, K. Watanabe, T. Taniguchi, D. Shi, Q. Zhang, and G. Zhang, Phys. Rev. B **97**, 235145 (2018).

[39] L. Du, Y. Zhao, Z. Jia, M. Liao, Q. Wang, X. Guo, Z. Shi, R. Yang, K. Watanabe, T. Taniguchi, J. Xiang, D. Shi, Q. Dai, Z. Sun, and G. Zhang, Phys. Rev. B **99**, 205410 (2019).

[40] C. M. Chow, H. Yu, A. M. Jones, J. Yan, D. G. Mandrus, T. Taniguchi, K. Watanabe, W. Yao, and X. Xu, Nano Lett. **17**, 1194 (2017).

[41] X. Hu, J. Zheng, and Z. Ren, Front. Phys. **13**, 137302 (2018).

[42] H. Hahn and W. Nickels, Z. Anorg. Allg. Chem. **314**, 307 (1962).

[43] R. Kniep, A. Wilms, J. Beister, and K. Syassen, Z. Naturforsch. B **36**, 1520 (1981).

[44] L. Wang and S. J. Hwu, Chem. Mater. **19**, 6212 (2007).

[45] K. M. Beck, W. R. Wiley, E. Venkatasubramanian, and F. Ohuchi, Appl. Surf. Sci. **255**, 9707 (2009).

[46]Y. Huo, J. Zhang, M. Miao, and Y. Jin, Appl. Catal. B **111–112**, 334 (2012).

[47]R. Loudon, Adv. Phys. **50**, 813 (2001).

[48]J. Bardeen, L. N. Cooper, and J. R. Schrieffer, Phys. Rev. **108**, 1175 (1957).

[49]M. Balkanski, R. F. Wallis, and E. Haro, Phys. Rev. B **28**, 1928 (1983).

[50]A. Raja, M. Selig, G. Berghäuser, J. Yu, H. M. Hill, A. F. Rigosi, L. E. Brus, A. Knorr, T. F. Heinz, E. Malic, and A. Chernikov, Nano Lett. **18**, 6135 (2018).

[51]M. B. Gisbert, D. A. Penares, J. Suh, F. Hidalgo, R. Abargues, P. J. R. Cantó, A. Segura, A. Cros, G. Tobias, E. Canadell, P. Ordejón, J. Wu, J. P. M. Pastor, and J. F. S. Royo, Nano Lett. **16**, 3221 (2016).